RSC Advances

PAPER

View Article Online
View Journal | View Issue

Cite this: *RSC Adv.*, 2026, **16**, 2671

Green synthesized ZnO nanocatalysts for rapid and effective visible-light degradation of industrial dyes

Toton Sarkar and Ashis Bhattacharjee †*

Synthetic dyes from industrial sources, particularly textiles, are major contributors to water pollution due to their non-biodegradable and toxic nature, posing serious environmental and health hazards. Semiconductor metal oxide nanomaterials have emerged as promising photocatalysts for dye degradation, owing to their activity, stability, and tunable structural–electronic properties. This study explores the visible-light-driven photocatalytic degradation of two hazardous dyes—Rose Bengal (RB) and Methylene Blue (MB)—using green-synthesized ZnO nanoparticles (NPs). The NPs were prepared *via* an eco-friendly route employing *Tabernaemontana divaricata* flower extract, producing three distinct samples: ZnO0 (17.5 nm), ZnO10 (20.8 nm), and ZnO15 (23.3 nm). Photocatalytic performance was evaluated under varying crystallite sizes, pH, catalyst dosages, and temperatures. Results revealed that activity increased with larger crystallite size, higher catalyst dosage, and elevated temperature, attributable to enhanced surface reactivity and reduced charge carrier recombination. ZnO15 achieved the highest efficiencies—99.14% (RB) and 99.42% (MB) degradation within 90 min—under optimized conditions, with rate constants of 0.07195 min^{-1} and 0.06922 min^{-1}, respectively. The degradation followed pseudo-first-order kinetics according to the Langmuir–Hinshelwood model. Optimal RB degradation occurred at pH 6, whereas MB degradation peaked at pH 10, reflecting the influence of electrostatic interactions between dye molecules and the ZnO surface. Scavenger experiments indicated that hydroxyl radicals were the dominant reactive species for RB degradation, while photogenerated holes played the key role in MB degradation. ZnO15 maintained significant activity over five successive cycles, suggesting good reusability. This work demonstrates that green-synthesized ZnO is an efficient photocatalyst for dye degradation under visible light and systematically assesses the influence of crystallite size, pH, catalyst loading, and temperature. While promising for wastewater treatment applications, further studies are needed to validate performance in complex effluents and under long-term operational conditions.

Received 4th November 2025
Accepted 19th December 2025

DOI: 10.1039/d5ra08475j

rsc.li/rsc-advances

1. Introduction

Water pollution from synthetic dyes, particularly from the textile industry, has become a major global concern, with an estimated 10–15% of dyes released untreated into natural water bodies. This poses severe threats to aquatic life,[1,2] human health,[3,4] and entire ecosystems.[5–8] These dyes are typically non-biodegradable, possess complex molecular structures, and can cause serious health problems, including skin and eye irritation,[9–12] as well as potential genotoxic, mutagenic, and cytotoxic effects and are believed to possess risks, including genotoxicity, mutagenicity, and even cytotoxicity.[13–16] To combat this issue, semiconductor metal oxide nanomaterials have emerged as promising candidates for dye degradation due to their chemical stability, large surface area, and strong photocatalytic activity.[17–26] The photocatalytic performance of such nanomaterials is influenced by factors including atomic structure, surface area, and electronic configuration.[27] Zinc Oxide (ZnO), a prominent II–VI n-type semiconductor with a direct band gap of 3.37 eV, offers several advantages: abundance, non-toxicity, and exceptional stability against energy radiation, wet electrochemical etching, and mechanical abrasion. It exhibits strong UV absorption, high durability, and a long operational lifespan, making it suitable for a wide range of applications.[28–31] These include photocatalysis,[32] spintronics,[33] gas sensor,[34] biomedicines,[35] rubber and plastic fillers,[36] luminescence,[37] UV-blocking agents,[38] solar cells,[39] antiviral coatings,[40] and nanopriming.[41] ZnO's high surface reactivity—attributable to its abundant defect states—makes it an economical and efficient photocatalyst for solar-driven environmental remediation.[42,43]

Various physical and chemical methods—such as hydrothermal, solvothermal, sonochemical, sol–gel, microemulsion, thermal decomposition, microwave irradiation, direct

Department of Physics, Visva-Bharati University, Santiniketan–731235, India. E-mail: ashis.bhattacharjee@visva-bharati.ac.in

† Present Address: Vice-Chancellor, University of Gour Banga, Malda, India.

precipitation, and laser ablation—are widely used to synthesize ZnO nanoparticles (NPs), enabling precise control over their shape, size, and properties.[44] However, these techniques often require lengthy reaction times and rely on costly, environmentally hazardous chemicals. In contrast, green synthesis has gained considerable attention for its eco-friendly and cost-effective nature.[44,45] This approach employs microorganisms (*e.g.*, bacteria, yeast, fungi, algae) and plant extracts derived from leaves, flowers, roots, and stems.[46] The phytochemicals in these extracts—such as terpenoids, flavonoids, phenolic compounds, aldehydes, and alkaloids—act as reducing agents to convert metal ions into NPs, while also serving as capping and stabilizing agents that control the final particle morphology.[46,47] By eliminating toxic reagents, green synthesis aligns with sustainable development goals and represents a promising avenue for applications such as dye degradation, as summarized in Table 1.

Dyes typically exhibit a wide range of structural variations, making it difficult to classify them based on a single parameter. However, dyes are categorized into various groups and classes based on their structure and source. The chemical structure of the dye determines both its colour and properties. Azo dyes are thought to be the most diverse group of colourants, accounting for more than half of all industrial dyes.[60] Azo dyes are mainly classified into cationic and anionic dyes. Among them Rose Bengal is the anionic dye whereas Methylene Blue is cationic dye. Rose Bengal (RB) is famous for its application in textiles, photochemistry, and dyeing. Industrial dyes like RB and MB are persistent water pollutants that are toxic and resistant to conventional treatment methods. Sako and his colleagues[61,62] investigated the toxic effects of RB. While substantial progress has been made in dye degradation techniques, studies specifically focusing on RB degradation remain limited. Additionally, previous researches reports indicate prolonged degradation times for RB. Bhar *et al.*[63] explored the degradation of RB using nanocrystalline FeS_2 thin films, achieving 84% dye degradation in 300 min. Farbod and Khademalrasool[64] investigated RB degradation with TiO_2 nanomaterials, achieving complete removal in 210 min. Likewise, Vignesh *et al.*[65] reported 85% degradation in 150 min using Ag-doped SnO_2 nanomaterials modified with curcumin. Given the persistent presence of RB in wastewater, there is a pressing need to eliminate it effectively. MB is utilized in machinery involved in cotton, wool, and fabric dyeing. These industries also use MB as a redox indicator along with colouring paper and even hair.[66] In comparison to RB, MB is reported to take longer time to degrade and requires higher dye to catalyst ratio for degradation. Khan *et al.*[66] studied the toxic effect of MB, and Kumar *et al.*[67] studied the degradation of MB. Kadam *et al.* examined the degradation of MB and reported 97.57% removal of the dye solution in 150 min by using thin

Table 1 Photocatalytic activity of green synthesized ZnO nanomaterials of various size below 30 nm[a]

Size (nm)	Dye	Dye used	Catalyst used	Dye to catalyst ratio	Maximum degradation (%)	Rate constant, k (min^{-1})	Light irradiation time (min)	Ref.
9.96	MB	50 mg L^{-1}	0.6 mg mL^{-1}		81.76	0.0207	90	48
12.62	MG	200 mL 10 ppm	10 mg	0.2	85	0.00799	240	49
14.54	MB	50 mg L^{-1}	0.6 mg mL^{-1}		77.18	0.0185	90	48
14.81	MB	12 mg mL^{-1}	30 mg		55	0.0021	200	50
17.96	MB	50 mg L^{-1}	0.6 mg mL^{-1}		69.28	0.0141	90	48
18.98	MB	10 ppm	50 mg		60	—	30	51
19	MB	15 mL 100 ppm	15 mg	1.5	92	0.0087	300	52
20.26	MB	50 mL 5 ppm	20 mg	0.25	95.1	0.0069	240	53
21	MB	12 μM L^{-1}	0.5 g L^{-1}		91.0	0.019	120	54
22	MB	12 μM L^{-1}	0.5 g L^{-1}		81.5	0.012	120	54
22.2	MB	15 ppm	100 mg		73.44	0.0129	90	55
23.67	MB	150 mL 20 μM L^{-1}	10 mg	0.096	98.29	0.0309	80	56
23.67	MO	150 mL 20 μM L^{-1}	10 mg	0.096	86.65	0.0130	100	56
25	MB	20 mL 5 ppm	15 mg	0.007	27.2	0.0241	90	57
25.8	MB	15 ppm	100 mg		81.92	0.0175	90	55
27.83	MO	15 ppm	40 mg		83.17	0.0154	120	58
28.12	MB	50 mL 10^{-5} M L^{-1}	5 mg	0.032	98.5	—	120	59
17.5, 20.8, 23.3	MB	100 mL 10 ppm	30, 45, 60 mg	0.016, 0.022, 0.033	99.42	0.06922	90	Present work
17.5, 20.8, 23.3	RB	100 mL 10 ppm	30, 45, 60 mg	0.016, 0.022, 0.033	99.14	0.07195	90	Present work

[a] (MB-methylene blue, MG-malachite green, MO-methyl orange, RB – Rose Bengal).

films of Ag nanomaterials.[68] Mahalingam *et al.* achieved 97% removal of α-MoO_3 nanocomposites in 240 min.[69]

Conventional photocatalysts often degrade dyes slowly, requiring prolonged exposure or harsh conditions. There remains a need for efficient, eco-friendly, and cost-effective catalysts capable of rapid dye degradation under visible light. The present study addresses this gap by employing green-synthesized ZnO nanomaterials (17.5–23.3 nm) prepared using *Tabernaemontana divaricata* flower extract (TFE).[70,71] The novelty of this study lies in integrating a sustainable green synthesis with a systematic performance evaluation of ZnO nanocatalysts. Using *Tabernaemontana divaricata* flower extract, ZnO nanoparticles were prepared *via* an eco-friendly route that avoids hazardous chemicals while ensuring stability and functionality. These green-synthesized ZnO nanomaterials achieved rapid visible-light-driven degradation of Rose Bengal and Methylene Blue, with >99% removal within 90 minutes—significantly faster than previously reported studies, especially for Rose Bengal. The work further distinguishes itself by correlating crystallite size, pH, catalyst dosage, and temperature with catalytic performance, while scavenger experiments revealed distinct reactive species governing the degradation of anionic and cationic dyes. In addition, the catalyst displayed excellent reusability. Collectively, these findings establish a novel, efficient, and environmentally benign pathway for dye remediation, underscoring strong potential for real-world wastewater treatment under visible light.

2. Materials and methods

2.1 Materials

Potassium hydroxide (KOH, ≥84%) for pH control of reaction medium was brought from Merck L Sc. Pvt. (India) Ltd The organic dyes – Methylene Blue ($C_{16}H_{18}N_3SCI$) and Rose Bengal ($C_{20}H_2Cl_4I_4Na_2O_5$) used for photocatalytic studies were procured from Aldon Co. and Sigma-Aldrich, respectively. Photocatalytic experiments involving scavengers were executed with isopropyl alcohol (IPA) (≥99%), potassium dichromate ($K_2Cr_2O_7$) (≥99%) and ethylene diamine tetra-acetic acid di-sodium (EDTA-2Na) (≥99%) which are effective scavengers for the OH*, $O_2{}^{*-}$, and h^+ radicals, respectively.

The synthesis of ZnO nanomaterials by using *Tabernaemontana divaricata* flower extract (TFE) are reported by us earlier.[70] Fresh and clean *Tabernaemontana divaricata* flowers were sun-dried for four days and subsequently ground into a fine powder using a grinder. Ten grams of the powder were heated at 80 °C in 100 mL of distilled water for 15 minutes under constant stirring. The resulting mixture was cooled to room temperature and filtered repeatedly to remove any residual particulates. The obtained light-brown solution was designated as the *Tabernaemontana divaricata* flower extract (hereafter referred to as TFE) and stored under refrigeration for further use in nanoparticle synthesis.

For the synthesis of ZnO nanoparticles, the procedure followed a reported literature method. Initially, 0.01 M zinc acetate dihydrate was dissolved in 100 mL of distilled water and stirred continuously for 30 minutes to obtain solution A. Separately, 0.2 M KOH was dissolved in 100 mL of distilled water to prepare solution B. For the synthesis of pure ZnO (denoted as ZnO0), solution B was added dropwise to solution A under stirring, resulting in the immediate formation of a white suspension. The mixture was then heated at 80 °C for 1 hour to yield a white precipitate, which was subsequently collected, filtered, and washed several times with distilled water and acetone. The product was finally dried at 80 °C for 4 hours to obtain ZnO0.

For the green synthesis of TFE-capped ZnO nanoparticles, solutions A and B were prepared as described above. In a typical synthesis, 10 mL of TFE was added to solution A prior to the addition of solution B. The remaining steps were identical to those used for ZnO0. The resulting sample was designated as ZnO10. Similarly, other TFE-capped ZnO sample (ZnO15) was prepared using 15 mL of TFE. In all syntheses, the pH of the reaction medium was maintained at 11. The dried products were finely powdered using a mortar and pestle for subsequent characterization. The results obtained on characterization of these ZnO nanomaterials are reported by us earlier[70] and are also provided as SI.

For photocatalytic degradation study, those ZnO nanomaterials have been used. ZnO prepared without use of TFE is named as ZnO0 while those prepared in presence of 10 mL and 15 mL of TFE are termed as ZnO10 and ZnO15. The reported crystallite size value of ZnO0, ZnO10 and ZnO15 are 17.5, 20.8 and 23.3 nm, respectively.[70]

2.2 Photocatalysis

Different amounts of ZnO nanoparticles were added in 100 mL 10 ppm aqueous solutions of dye (MB/RB) at different steady temperatures and different solution pH. To ensure adsorption of dye on the nanomaterials surface, the solution was stirred in dark for 1 h. Then the solution was exposed to light source of Newport Corporation, USA. The degradation of the solution was tracked by collecting the sample solutions at every 15 min intervals and this solution was centrifuged to remove the ZnO nanoparticles. This aqueous remaining dye solution absorbance was measured using a Beckman DU®720 UV/Vis spectrophotometer. For scavenger tests initially 1 mM L^{-1} aq. solutions of $K_2Cr_2O_7$, IPA, and EDTA-2Na were prepared individually. Different amounts of scavenger solutions (3 mL and 6 mL) were added to the dye solution containing photocatalyst and RB/MB.

The recorded absorption spectra were analyzed to determine % of photocatalytic degradation of RB/MB dye over time using following equation:

$$\%\ \text{Degradation} = (C_0 - C)/C_0 \quad (1)$$

where C_o represents the initial concentration of the MB/RB solution, and C is the concentration of the MB/RB solution after a given period of light exposure (t). The reaction kinetics of dye degradation can be described by the equation:

$$(C/C_0) = \exp(-kt) \quad (2)$$

where C_0 represents the initial dye concentration, C is the concentration at a specific time t (min), and k (min^{-1}) is the reaction rate constant, following the Langmuir–Hinshelwood model.[72] (The photodegradation process of the present dye molecules fits with the pseudo-first-order kinetics model). The rate constant, which quantifies the speed of reaction, reflects how rapidly the dye molecules decompose under photocatalytic conditions. The half-life ($t_{1/2}$), which represents the time needed for the initial dye concentration to decrease by 50%, can be calculated using equation as follows:

$$t_{1/2} = \ln(2)/k = 0.693/k \quad (3)$$

3. Results and discussion

3.1 Optical absorption study to visualize photocatalytic dye degradation

Time-dependent absorption spectra were recorded up to 90 min under different experimental conditions: (i) dye solution kept in dark without catalyst, (ii) dye solution exposed to light without catalyst, and (iii) dye solution exposed to light with catalyst (See Fig. S1(a–f)). The observed intensities of the spectra obtained under these conditions are summarized in Fig. 1. This figure shows the extent of dye degradation observed under the above said different conditions as a function of time. There is no appreciable variation observed in the relative concentration of the dyes when exposed to light without the catalyst or even when the catalyst is present in the absence of light, indicating no degradation reaction occurred. (Small changes observed in C/C_0 values over time in Fig. 1 lie within experimental errors.)

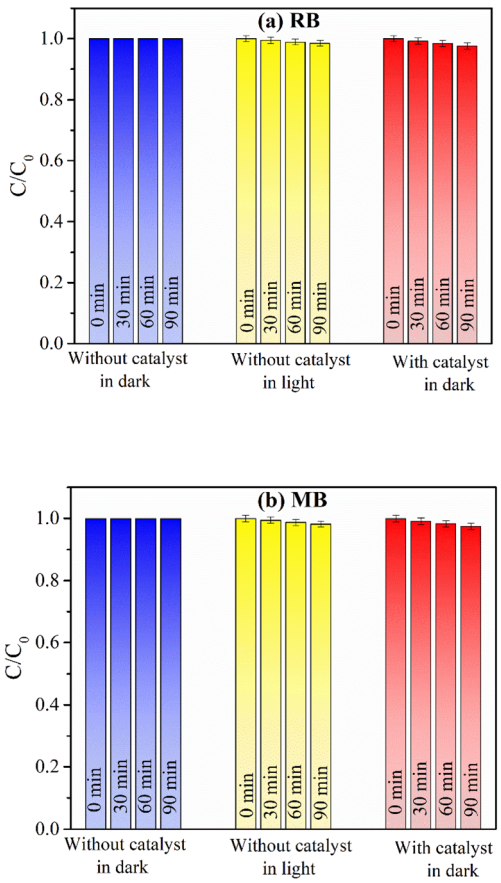

Fig. 1 Degradation observed for (a) RB and (b) MB under different reaction conditions with time.

However, a marked decrease in dye concentration is observed when the ZnO nanomaterials are present under light irradiation, as presented in Fig. 2. Time-dependent absorption spectra recorded up to 90 min of light irradiation of dye solutions catalyzed by ZnO0, ZnO10, and ZnO15 nanomaterials for RB are presented in Fig. 2(a–c), while those for MB are presented in Fig. 2(d–f). These figures clearly illustrate a regular decrease in the intensity of the characteristic absorption peaks for RB at 547 nm and MB at 660 nm over time. This observation suggests that the primary mechanism behind the dye degradation is the photocatalytic activity of ZnO nanomaterials rather than simple catalysis or adsorption on the catalyst surface.

The rate constants for the photocatalytic degradation of dyes using ZnO0, ZnO10, and ZnO15 were calculated to be 0.01309, 0.01732 and 0.02241 min^{-1} for RB, and 0.01158, 0.01387 and 0.01596 min^{-1} for MB in room temperature with pH value 6, respectively. The estimated first-order reaction rate constants (k), obtained using eqn (2), are shown in Tables 2 and 3, along with the half-life ($t_{1/2}$) calculated using eqn (3). These values correspond to different catalyst sizes, solution pH values, catalyst amounts, and temperatures.

3.2 Effect of crystallite size

The effect of crystallite size on photocatalytic efficiency was examined by monitoring the time-dependent degradation of dyes under visible light irradiation using ZnO0, ZnO10, and ZnO15, as presented in Fig. 2(g and h). This demonstrates the variation of C/C_0 with time derived from the results shown in Fig. S1 and 2(a–f). The solid curves are fits to the eqn (2). Tables 2 and 3 summarize the extent of RB and MB dye degradation observed after 90 min of light irradiation obtained with ZnO0, ZnO10, and ZnO15 as photocatalysts. Tables 2 and 3 show that ZnO15 with larger crystallite size exhibited superior performance, achieving 84.86% dye degradation with rate constant 2.24×10^{-2} min^{-1} for RB and 75.47% degradation with rate constant 1.59×10^{-2} min^{-1} for MB, compared to ZnO0 and ZnO10 under identical experimental conditions at room temperature.

Fig. 2(i) summarizes the variation of maximum degradation of RB and MB dye and the rate constant values with the crystallite size of the catalyst, which shows that the larger crystallite size ZnO15 enhances the photocatalytic performance. This agrees with the findings from Ravbar *et al.*,[73] Soto-Robles *et al.*[55] and Taha *et al.*.[74] The increased photocatalytic activity with increasing crystallite size is attributed to the surface properties, particularly the specific surface area and band gap energy of ZnO nanomaterials. In this mechanism, the generated holes interact with hydroxyl groups of the surface to produce surface-bound hydroxyl radicals. At the same time, photoexcited electrons are captured by surface oxygen deficiencies, thereby

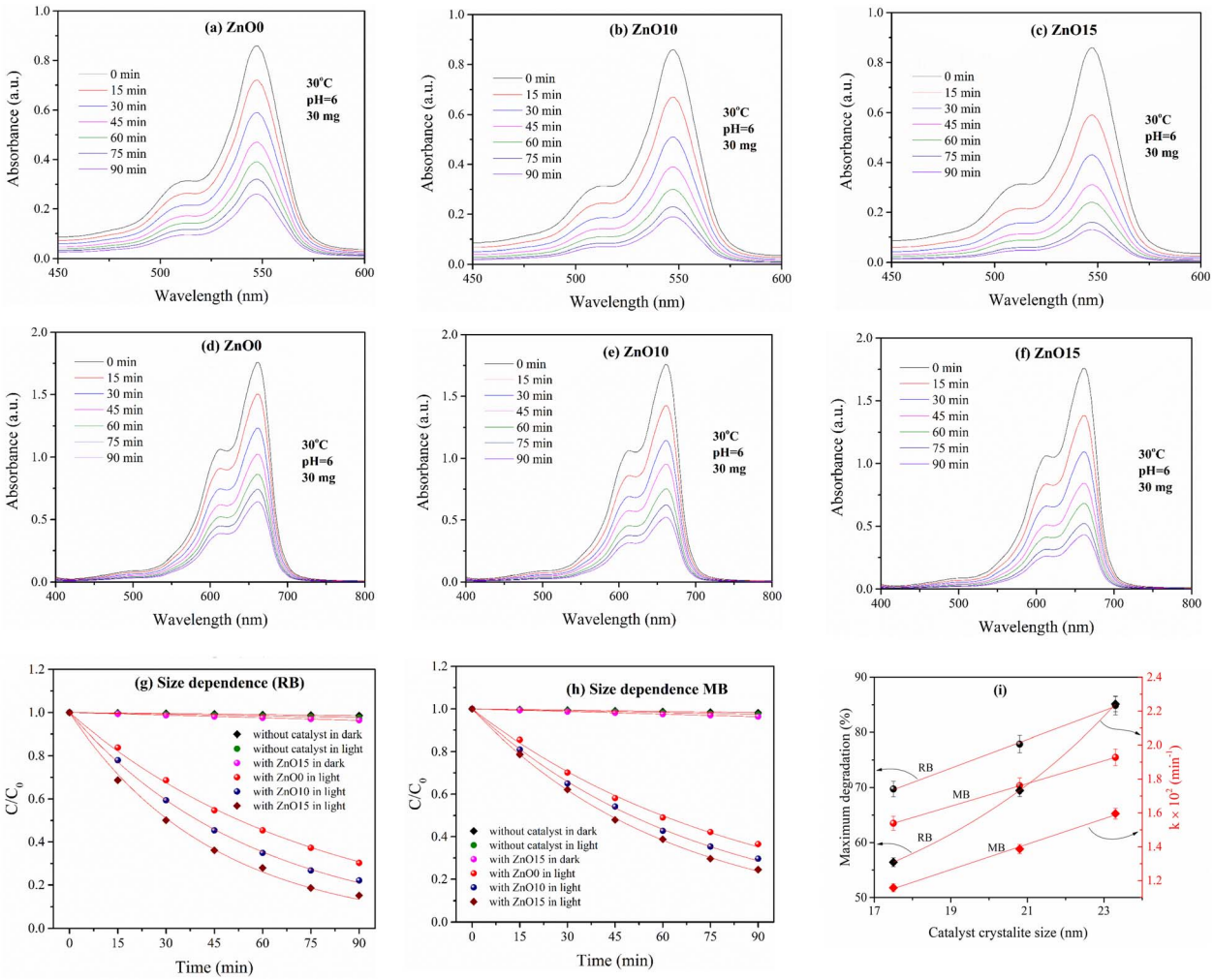

Fig. 2 (a–c) and (d–f) Absorption spectra of RB and MB solutions in presence 30 mg of ZnO0, ZnO10, and ZnO15 at room temperature and solution pH 6 after different durations of irradiation of light; (g and h) photodegradation of RB and MB at room temperature under various conditions, (R^2 value of 0.99 indicates the high quality of fit with eqn (2) for all experimental data); (i) variation of the maximum degradation of RB and MB and rate constant values with crystallite size of catalyst.

reducing the recombination of photogenerated charge carriers. Intensity-modulated photocurrent and photovoltage measurements further validated this concept, showing that the recombination rate of photogenerated holes decreases as crystallite size increases.[75] These indicate larger crystallite size of ZnO can reduce charge carrier recombination, enhancing photocatalytic performance.

To see the role of crystallite size of ZnO nanomaterials on the photocatalytic dye degradation, comparison of some relevant literature reports has been performed in Table 1. This table

Table 2 Max. degradation, reaction rate and half-life time of RB values for different size, pH of solution, amount of catalyst and reaction temperature

Sample	Size	Solution pH	Amount (mg)	Temperature (°C)	Max degradation (%)	Reaction rate, k (min^{-1})	R^2	$t_{1/2}$ (min)
ZnO0	17.5	6	30	30	69.73	0.01309	0.998	52.94
ZnO10	20.8	6	30	30	77.88	0.01732	0.997	39.21
ZnO15	23.3	6	30	30	84.86	0.02241	0.997	30.92
ZnO15	23.3	8	30	30	74.53	0.01520	0.999	45.59
ZnO15	23.3	10	30	30	64.12	0.01137	0.999	60.94
ZnO15	23.3	6	45	30	90.68	0.02756	0.999	25.14
ZnO15	23.3	6	60	30	96.50	0.03872	0.999	17.89
ZnO15	23.3	6	60	50	98.78	0.05302	0.999	13.07
ZnO15	23.3	6	60	70	99.14	0.07195	0.999	9.63

Table 3 Max. degradation, reaction rate and half-life time of MB values for different size, pH of solution, amount of catalyst and reaction temperature

Sample	Size	Solution pH	Dose (mg)	Temperature (°C)	Max. degradation (%)	Reaction rate, k (min^{-1})	R^2	$t_{1/2}$ (min)
ZnO0	17.5	6	30	30	63.49	0.01158	0.998	59.84
ZnO10	20.8	6	30	30	70.33	0.01387	0.999	49.96
ZnO15	23.3	6	30	30	75.47	0.01596	0.999	43.42
ZnO15	23.3	8	30	30	79.32	0.01798	0.999	38.54
ZnO15	23.3	10	30	30	83.88	0.02127	0.998	32.58
ZnO15	23.3	10	45	30	91.44	0.02841	0.999	24.39
ZnO15	23.3	10	60	30	96.57	0.03582	0.999	19.34
ZnO15	23.3	10	60	50	98.85	0.05728	0.999	12.09
ZnO15	23.3	10	60	70	99.42	0.06922	0.999	10.01

compares dye to catalyst weight ratio, irradiation time, rate constant and maximum degradation values reported for different dye degradation by green-synthesized zinc oxide nanomaterials of various crystallite sizes reported in the literature. Fig. 3 displays variations of the degradation rate depending on the crystallite size where the k values increase with crystallite size. Evidently, the rate at which the dyes degrade is significantly influenced by the crystallite size of the nanomaterials. These findings are consistent with the present experimental results.

3.3 Effect of solution pH

As the effectiveness of dye degradation strongly depends on the pH of the reaction medium,[76,77] the influence of pH in degradation of RB and MB dyes has been studied. Fig. 4(a and b) compare the absorption spectra recorded after 90 min of light irradiation for RB and MB at different pH values, while maintaining a constant amount of catalyst and solution temperature, together with the spectra obtained without the catalyst (see Fig. S2 for all absorption spectra). This clearly illustrates the impact of pH on dye degradation. Absorption spectra recorded after 90 min of light irradiation for RB and MB at various pH values, with a constant catalyst amount and solution temperature are displayed in Fig. 4(c and d). Solid curves indicate the fits to eqn (2) and the fitted value are presented in Tables 2 and 3.

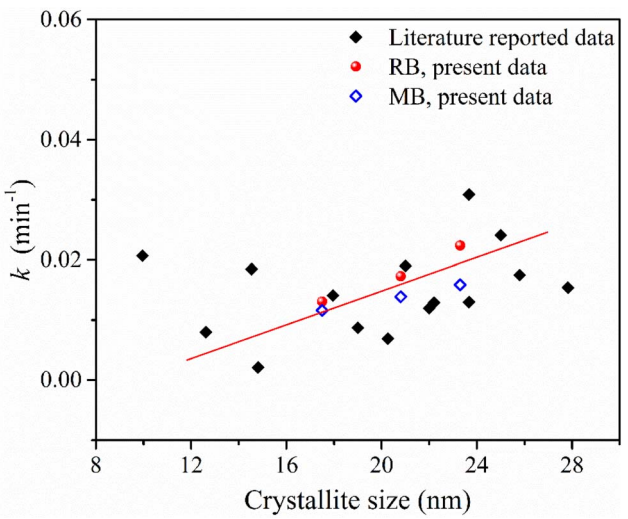

Fig. 3 Variation of rate constant with crystallite size for photocatalytic degradation of MB and RB by ZnO. The solid line is a guide to the eye.

Fig. 4(e and f), show the variation of maximum dye degradation after 90 min and the corresponding rate constant at various pH levels for a fixed amount of catalyst at room temperature. The findings show that as the pH increases, the rate constant and degradation efficiency for RB decrease, whereas an opposite trend is observed for MB. Tables show that at pH = 6, RB exhibited superior performance, achieving 84.86% dye degradation with a rate constant of 2.24×10^{-2} min^{-1}. In contrast, for MB, the optimal performance is observed at pH = 10, with 83.88% dye degradation and a rate constant of 2.12×10^{-2} min^{-1}. As, the amount of catalyst and dye are kept constant, the observed change in dye degradation with increasing pH can be attributed solely to the effect of pH in the reaction medium. Similar trends were noticed by Shubha *et al.*,[78] Kazeminezhad *et al.*,[79] Isai *et al.*[80] and Irede *et al.*[81]

The pH-dependent RB and MB dye degradation can be explained by their nature as anionic and cationic dyes, respectively. As the pH increases, the repulsive forces between the catalyst surface and the RB dye molecules become stronger, leading to a reduction in the dye degradation rate. On other hand opposite behavior is shown by MB dye molecules.[82] The higher rate of MB degradation at alkaline pH of the solution suggests that the negatively charged surface of the catalyst promotes electrostatic attraction. Higher degradation of the MB dye occurs rapidly under alkaline conditions. Initially, MB degradation progresses slowly because of the dye's acidic pH, which inhibits the creation of hydroxyl radicals. Under alkaline conditions (pH 10), the MB dye solution generates an excess of hydroxyl and superoxide radicals, significantly enhancing the degradation process within a short time. According to Alkaykh *et al.*, the production of protons in the dye degradation process reduces the degradation rate.[83] According to Nosaka and Nosaka,[84] radical production is directly proportional to photocatalytic degradation efficiency. At neutral and acidic pH levels (7 and 6), the high concentration of protons interacts with hydroxyl radicals, forming water molecules, as described by

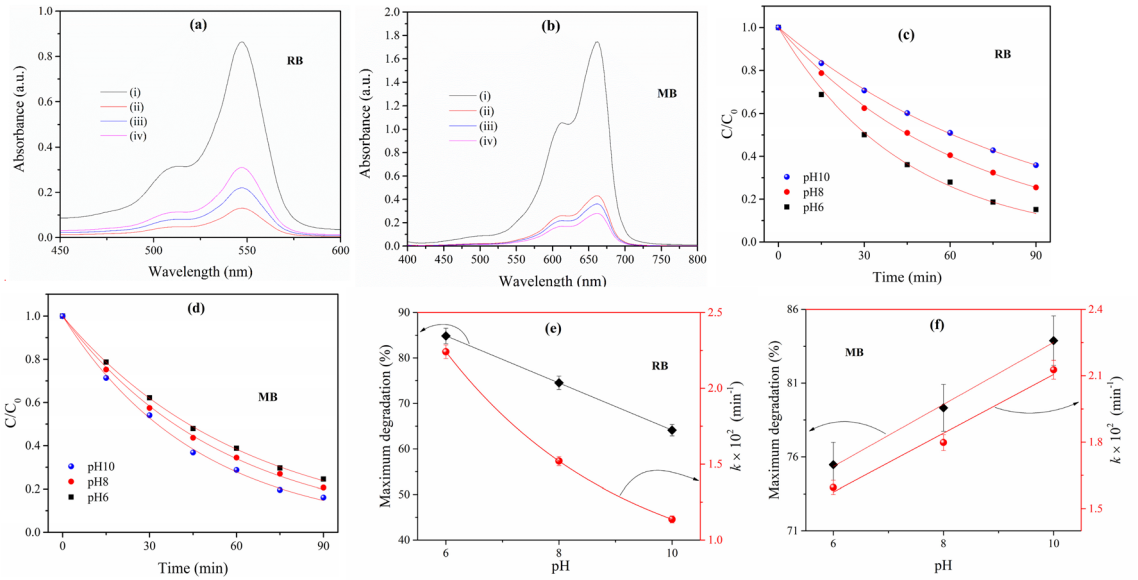

Fig. 4 Photocatalytic degradation of RB and MB under different pH of the dye solution using 30 mg of ZnO15 as the photocatalyst at room temperature: (a and b) absorption spectra recorded after 90 min for dye solutions (i) without catalyst, (ii) at pH 6, (iii) at pH 8, and (iv) at pH 10; (c and d) time-dependent photodegradation of dye solutions at different pH (solid curves indicate the fits to eqn (2)); (e and f) dependence of the maximum dye degradation and rate constants as a function of the pH values.

Nasikhudin *et al.*[85] and Zhang *et al.*.[86] This reaction reduces the availability of hydroxyl radicals, thereby slowing the degradation process. In contrast, the dye solution exhibiting a basic nature at pH 10 supports the generation of abundant hydroxyl and superoxide radicals, which accelerates the degradation process efficiently.

It is known that pH of zero point charge (pHZPC) is a key factor in the cases of adsorption, catalysis, wastewater treatment, and material science as it helps to characterize the surface properties of materials and predict their behaviour in various applications. Experimental pHZPC data would provide a more quantitative basis for interpreting the pH-dependent results. However, in the present study, authors did not perform direct measurement of pHZPC for the green-synthesized ZnO nanoparticles, but the same will be addressed in future work. Instead, the influence of pH on photocatalytic degradation has been systematically investigated, and the observed trends in degradation efficiency (optimal pH = 6 for Rose Bengal and pH = 10 for Methylene Blue) are consistent with the expected electrostatic interactions between the dyes and ZnO surface reported in literature.

3.4 Effect of dye dosage

To assess the influence of catalyst dose on dye degradation, the photocatalytic dye degradation is studied with varying amounts of ZnO15 catalyst at 30 °C under pH 6 for RB, while the degradation of MB dye was examined under pH 10 under the same temperature. Absorption spectra recorded after 90 min of light irradiation for RB and MB at varying amounts of ZnO15 catalyst for a fixed pH at room temperature are displayed in Fig. 5(a and b). The time-dependent spectra are shown in Fig. S3. In Fig. 5(c and d) time dependence of RB and MB dye degradation after 90 min light irradiation at various amounts of catalyst is shown for a fixed pH at room temperature, respectively. Solid curves indicate the fits to eqn (2) and the fitted value are presented in Tables 2 and 3. These Table show that 60 mg of ZnO15 exhibited superior performance, achieving 96.50% dye degradation with rate constant 3.87×10^{-2} min^{-1} for RB and 96.57% degradation with rate constant 3.58×10^{-2} min^{-1} for MB. These outcomes are achieved under identical experimental conditions at room temperature in comparison to 30 mg and 45 mg of ZnO15.

Fig. 5(e and f) shows the quantitative relationship between the photocatalyst dose and the percentage of dye degraded after 90 min irradiation of light at room temperature for RB at pH = 6 and MB at pH = 10, along with the corresponding rate constant values. This result indicates a linear increase in maximum degradation and rate constant with larger dose of catalyst, previous studies have reported similar trends.[81] Increasing the catalyst quantity enhances the total available surface area, which promotes greater adsorption of dye molecules. This improved adsorption capacity facilitates more efficient interactions between the dye molecules and the catalyst, leading to enhanced degradation. As the photocatalyst amount increases, more active sites become available on its surface for catalytic reactions.[82] This larger number of active sites promotes the generation of additional photogenerated electron–hole pairs, which are necessary for creating hydroxyl radicals that drive the dye degradation process.[82] Consequently, increasing the quantity of photocatalyst results in a larger surface area, enhanced adsorption capacity, and an increased active sites number, all contributing to improved degradation efficiency of dye molecules in solution.

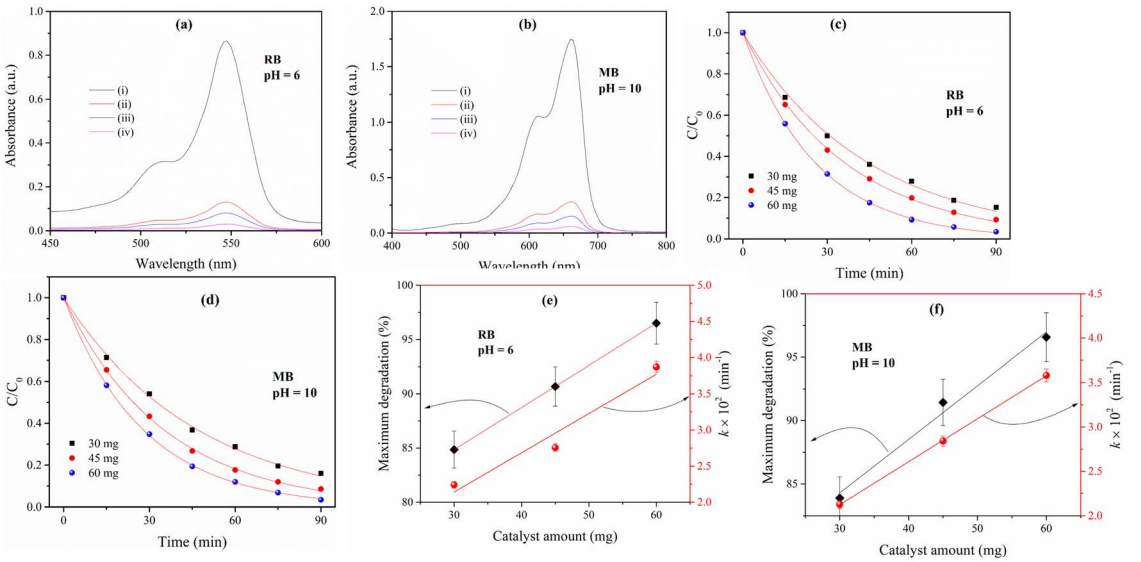

Fig. 5 Photocatalytic dye degradation using ZnO15 at room temperature and constant pH under different dose of catalyst: (a and b) absorption spectra of RB and MB solution after 90 min with varying dose of ZnO15—(i) no catalyst, (ii) 30 mg, (iii) 45 mg, (iv) 60 mg; (c and d) time-dependent photodegradation of RB and MB in the presence of different ZnO15 doses (solid curves represent fits to eqn. (2)); (e and f) variation of the maximum dye degradation and corresponding rate constant with dose of ZnO15.

3.5 Effect of solution temperature

To examine the effect of solution temperature on the dye degradation, RB (at pH = 6) and MB (at pH = 10) dye degradations are investigated using 60 mg of ZnO15 photocatalyst at varying temperatures −30 °C, 50 °C, and 70 °C. Absorption spectra recorded after 90 min of light irradiation for RB and MB at different solution temperature in presence of fixed amount of ZnO15 and pH are displayed in Fig. 6(a and b). See the time-dependent spectra in Fig. S4. In Fig. 6(c and d) time dependence RB and MB dye degradation 90 min light irradiation at different solution temperature in presence of fixed amount of ZnO15 and pH, respectively. Tables 2 and 3 show that a dye solution temperature of 70 °C exhibited superior performance, achieving 99.14% dye degradation with rate constant 7.19 × 10^{-2} min^{-1} for RB and 99.42% degradation with rate constant

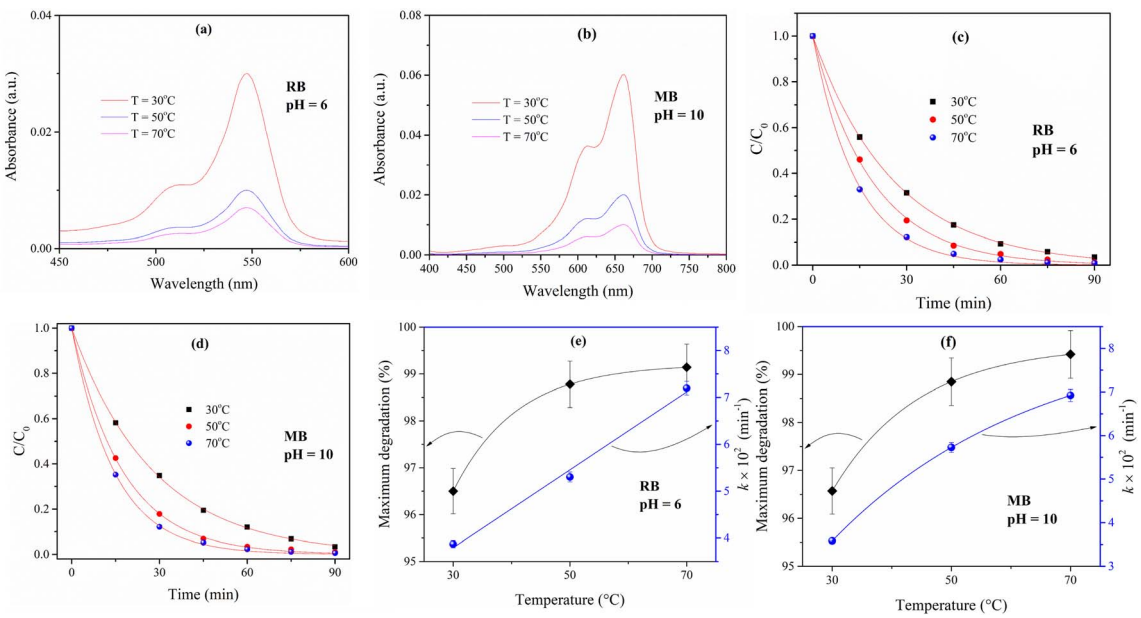

Fig. 6 Effect of temperature on photocatalytic dye degradation using 60 mg ZnO15 under constant pH: (a and b) absorption spectra RB and MB dye degradation after 90 min at different temperatures; (c and d) time-dependent photodegradation of RB and MB solutions at different solution temperatures (solid curves indicate the fits to eqn (2)); (e and f) changes in maximum dye degradation and rate constants as a function of solution temperature.

6.92×10^{-2} min^{-1} for MB. These outcomes are obtained under identical experimental conditions, in comparison to dye solution temperature of 30 °C and 50 °C.

Fig. 6(e and f) represent the quantitative relationship between the solution temperature and the degradation percentage of dye after 90 min light irradiation with a fixed catalyst amount for RB at pH = 6 and MB at pH = 10, along with the corresponding rate constant values. The observed trend demonstrates that both the degradation percentage and rate constant increase linearly with increasing solution temperature which in agreement with literature report.[81]

Notably, there are currently no temperature dependence studies in the literature on the of RB dye degradation with ZnO as a photocatalyst, to the best of our knowledge. However, there are some temperature dependence reports on the photocatalytic activity using hematite and bismuth ferrite as catalysts.[87–89] The improvement in degradation efficiency is apparent, and it is clear that higher temperatures speed up the degradation process. Specifically, both rate constant and degradation efficiency show an increase with temperature after 90 min of light irradiation. This type of photocatalytic behavior can be described by considering that increased temperature improves the mobility of the charge carrier and facilitate interfacial charge transfer enhancing the photocatalytic activity.[90,91] The influence of water temperature on titanium dioxide's photocatalytic activity was reported by Janus *et al.*.[92] As dye solution temperature rises, so does the amount of radical's hydroxyl in the water due to the increase in ionic product of water. Increase in efficiency is linked to an increase in the water's ionic product, which rises with temperature and raises the hydroxyl ion concentration. According to Meng *et al.*,[93] a higher reaction temperature substantially encourages dye molecule mobility, making it easier for the molecules to pass through the material's micropores. The ambient temperature dependent of the reaction rate constant can be understood by the fact that warmer temperatures offer more energy for the reactant molecules, which increases their kinetic energy. As result, number of collisions between catalyst and dye molecules increases, leading to an increased reaction rate, and hence higher dye degradation efficiency.

3.6 Mechanistic pathway of dye degradation

Fig. 7 presents a schematic diagram illustrating the photocatalytic mechanism of the synthesized zinc oxide nanoparticles. The mechanism of photocatalytic degradation of RB/MB dyes using ZnO as catalyst presumably involves an advanced oxidation process.[88,94] When photons are absorbed by the photosensitive dye (say, dye^0), these molecules shift to an excited singlet state (say, dye^1), followed by conversion to an excited triplet state (say, dye^2) through inter system.[88,94] The observed photodegradation of the dyes in the presence of semiconducting ZnO can be attributed to photocatalysis initiated by the semiconductor, with the proposed mechanism outlined below. Upon photo-excitation, electron (e^-) and hole (h^+) pairs are generated in the conduction and valence bands of the ZnO semiconductor, respectively. During this process, free electrons on the catalyst surface are excited from the valence band to the conduction band. These generated electrons interact with adsorbed O_2 molecules, leading to the formation of superoxide anion radicals ($O_2{}^{*-}$), which subsequently produce HO_2^* in presence of water. Meanwhile, the holes can generate hydroxyl radicals (OH^-) when they interact with surface OH^- groups.[95–97] Additionally, the O_2^- radicals can act as oxidizing agents and serve as an extra source of hydroxyl radicals. During the reaction, hydrogen peroxide (H_2O_2) is produced as an intermediate product, which can absorb electrons to generate OH* radicals. Another potential pathway involves a Fenton-like reaction, where Zn^{2+} on the surfaces of zinc oxides under illumination, followed by a reaction between Zn^{2+} and H_2O_2 to generate (OH*) radicals.[98] It is important to note that, since only small quantities of radicals are involved in this study, the influence of photo-Fenton reaction is presumed to be minimal. These (OH*) and ($O_2{}^{*-}$) radicals have significant impact on degrading the (RB/MB) dye molecules by oxidizing them to their colourless leuco form and eventually to harmless compounds. Thus, ultimately, the reactive radicals interact with dye molecules, degrading them into non-toxic by products such as CO_2 and H_2O. Moreover, organic pollutants adsorbed on the photocatalyst surface can be directly oxidized.[99] In summary, the photocatalytic degradation process using ZnO encompasses both oxidative (*via* holes) and reductive (*via* electrons) pathways, which can be outlined as follows:[100]

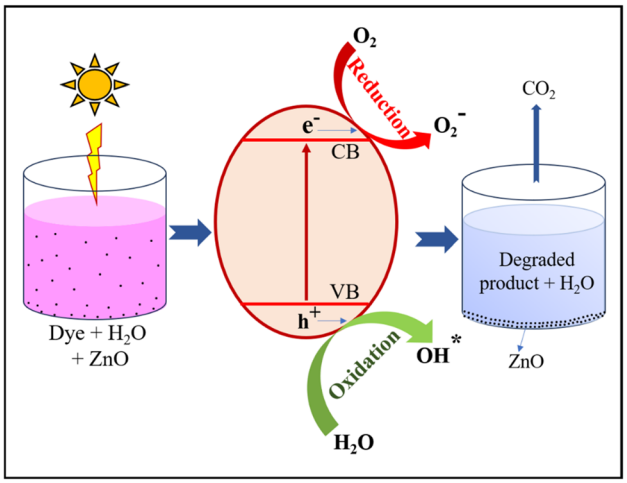

Fig. 7 Schematic diagram represents the photocatalysis mechanism.

$$dye^0 + h\nu \rightarrow dye^1$$

$$dye^1 \rightarrow dye^2 \text{ (inter system crossing)}$$

$$ZnO + h\nu \rightarrow ZnO\ (e^- + h^+) \text{ (electron–hole pair due to photoexcitation)}$$

$$O_2 + e^- \rightarrow O_2{}^{*-} \text{(formation of superoxide radical anion)}$$

$$h^+ + H_2O \rightarrow H^+ + OH^- \text{ (neutralization of } OH^- \text{ group into OH by hole)}$$

$$O_2^{*-} + H^+ \rightarrow HO_2^*$$

$$HO_2^* + HO_2^* \rightarrow H_2O_2 + O_2$$

$$H_2O_2 + h\nu \rightarrow 2OH^*$$

$$OH^* + dye^2 \rightarrow \text{Leuco form of dye}$$

Leuco form of dye → degraded product + CO_2 + H_2O. ESR/EPR-based studies are planned as part of our future work to further validate and expand upon the mechanistic conclusions.

The morphological differences among the ZnO0, ZnO10, and ZnO15 catalysts significantly influence their photocatalytic performance. Although their particle sizes are similar, variations in band gap energy affect both dye adsorption and light absorption. Additionally, the kinetics of the electron–hole pair generation and recombination processes play a crucial role.[101] Imperfections in the crystal structure notably impact the rates of electron–hole recombination, while resistance during charge transfer at the interface between the catalyst and dye further contributes to differences in degradation efficiency. Previous studies[70] utilizing room-temperature photoluminescence support this observation, indicating that factors such as catalyst morphology, specific surface area, crystal defects, and challenges in efficient interfacial charge transfer are all important.[102] However, further research under controlled experimental conditions is needed to identify the exact underlying mechanisms.

3.7 Radical scavenging experiments

To explore the role of reactive species in the photodegradation of RB and MB dye, a radical trapping or scavenger activity study is performed. To determine the reactive species, present during the photodegradation of RB dye, different scavengers were used. Fig. 8(a and b) indicates the scavenger activity in RB and MB dye solution in presence of ZnO15 nanoparticles, respectively. The scavengers trap the reactive species and decrease their production. Here, potassium dichromate ($K_2Cr_2O_7$), isopropyl alcohol (IPA), and ethylene diamine tetra acetic acid disodium (EDTA-2Na) are used as $O_2{}^{*-}$, OH*, and h^+ scavengers respectively, to examine their impact on the photodegradation of RB and MB dye. It is noted that without scavenger, the total degradation percentage of RB dye is 96.57% for 60 mg of ZnO15 catalyst at room temperature and medium pH 6. However, when 3 mL scavenger is added, the total degradation percentage reduces to 48.1% for $K_2Cr_2O_7$, 34.2% for IPA, and 61.3% for EDTA-2Na. This reduction suggests that these scavengers inhibit the degradation process by quenching reactive species responsible for dye degradation. With increasing of the scavenger amount to 6 mL, the degradation further reduces to 24.6%, 12.4%, and 37.8% for $K_2Cr_2O_7$, IPA, and EDTA-2Na, respectively. Thus, there is significant reduction in the photodegradation efficiency for RB dye using ZnO15 as photocatalyst

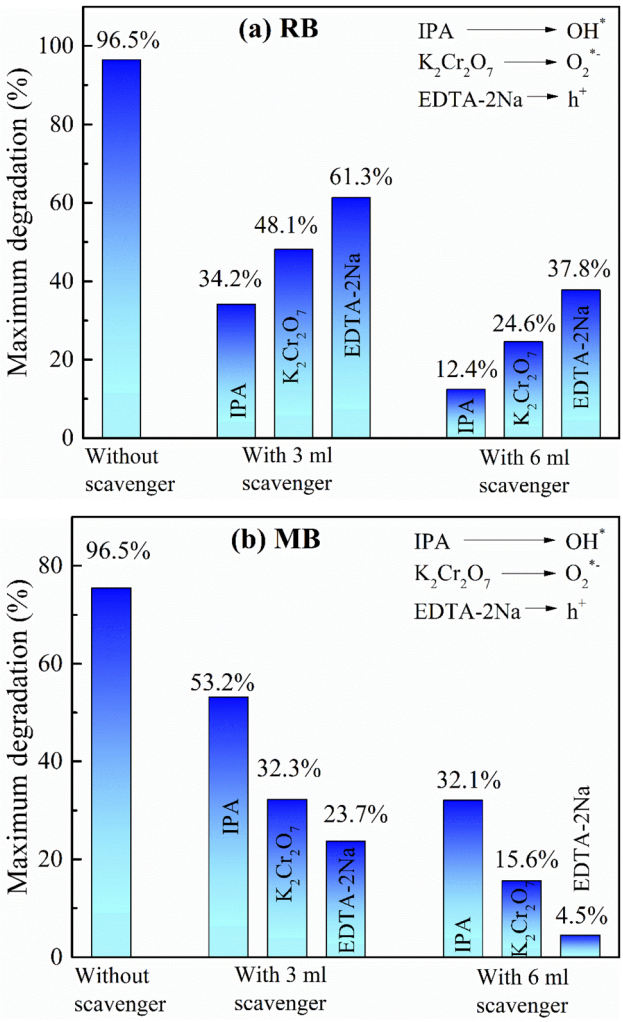

Fig. 8 Scavenger activity during photodegradation of (a) RB and (b) MB using 60 mg of ZnO15 catalyst at room temperature and pH 6.

in presence of these scavengers used, and the dye degradation efficiency decreases in the following order: IPA > $K_2Cr_2O_7$ > EDTA-2Na.

For MB dye, without scavenger, the total degradation percentage was 75.47% under the same conditions. However, the addition of 3 mL scavenger reduced the total degradation percentage to 32.3% for $K_2Cr_2O_7$, 53.2% for IPA, and 23.7% for EDTA-2Na. Increasing of the scavenger amount to 6 mL further reduced the degradation to 15.6%, 32.1%, and 4.5% for $K_2Cr_2O_7$, IPA, and EDTA-2Na, respectively. In this case, the order of efficiency reduction for MB dye was IPA < $K_2Cr_2O_7$ < EDTA-2Na.

The strongest inhibition of RB dye degradation occurred with IPA, indicating that among the reactive species (OH*, $O_2{}^{*-}$, and h^+), hydroxyl radical play the most significant role in the photodegradation of RB dye. In contrast, for MB dye, the strongest inhibition was observed with EDTA-2Na, suggesting that holes (h^+) are primarily responsible for the photodegradation of MB dye.

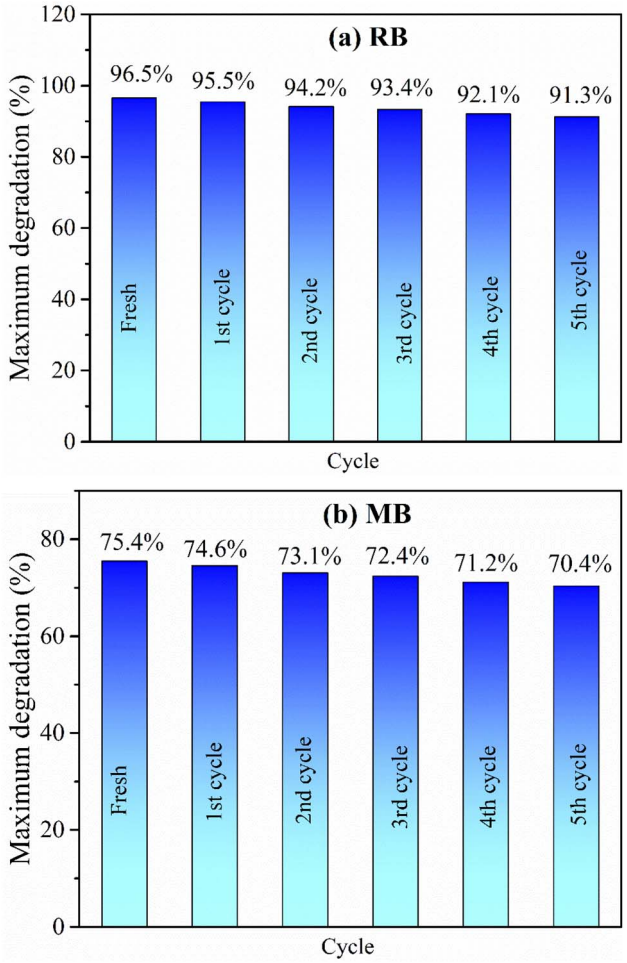

Fig. 9 Reusability of green-synthesized ZnO nanoparticles in the photodegradation of (a) Rose Bengal (RB) and (b) Methylene Blue (MB) using 60 mg of ZnO15 catalyst at room temperature and pH 6.

3.8 Recyclability of the photocatalyst

To assess the reusability of green-synthesized ZnO nanoparticles in the photodegradation of RB and MB dyes, experiments were conducted using a ZnO15 catalyst dosage of 60 mg in 100 mL of a 10 ppm dye solution with pH 6, with a reaction time of 90 min. After each cycle, the ZnO nanoparticles were recovered, thoroughly washed, and dried for reuse. Fig. 9 shows reusability of green-synthesized ZnO nanoparticles in the photodegradation of RB and MB using 60 mg of ZnO15 catalyst at room temperature and pH 6. Absorption spectra after 90 min light irradiation of RB and MB solution for five recycle with ZnO15 at room temperature are shown in SI Fig. S5. Over the course of five successive photodegradation cycles, only a slight reduction in catalytic efficiency was observed (see Fig. 9), demonstrating the stability of the ZnO NPs.

To verify any structural changes in the catalyst, powder XRD patterns of green-synthesized nanomaterials were collected and analyzed before and after photocatalysis (see SI). The similarity between the two XRD patterns, along with the consistency of the estimated parameters for both samples, confirmed that the green-synthesized nanomaterials used as a photocatalyst for dye degradation remained structural unchanged during repeated photocatalysis.

4. Conclusion

The present study demonstrates the potential of green-synthesized ZnO nanomaterials, fabricated using *Tabernaemontana divaricata* flower extract, as visible-light-driven photocatalysts for the degradation of two model dyes—Rose Bengal (RB) and Methylene Blue (MB). Systematic investigations revealed that dye degradation efficiency was significantly influenced by the crystallite size of the photocatalyst, solution pH, catalyst dosage, and reaction temperature. Among the three nanomaterials, ZnO15 (23.3 nm) exhibited the highest degradation efficiencies—up to 99.14% for RB and 99.42% for MB within 90 min of visible light irradiation. The reactions followed pseudo-first-order kinetics consistent with the Langmuir–Hinshelwood model, with optimal conditions identified as pH = 6 for RB and pH = 10 for MB. Scavenger experiments suggested that hydroxyl radicals were the dominant reactive species for RB degradation, whereas photogenerated holes played the major role in MB degradation. Temperature and catalyst dosage were also found to enhance the reaction kinetics by promoting charge carrier mobility, radical generation, and increasing active surface area. ZnO15 maintained photocatalytic activity over five cycles, indicating reasonable reusability.

This study was limited to two dyes in controlled aqueous solutions, and the findings may not fully represent the behaviour of industrial effluents containing mixed pollutants and competing ions. Extreme acidic conditions were not explored due to potential catalyst instability. Catalyst reusability was assessed only up to five cycles, and long-term durability under continuous operation remains to be evaluated. Future studies should therefore examine performance in real wastewater matrices, investigate mixed-dye degradation, and explore extended stability testing to further assess practical applicability.

Author contributions

Material preparation, major data collection and analysis were performed by TS. AB conceptualized the problem and designed the study. The first draft of the manuscript was written by TS and finalized by AB. All authors reviewed the final manuscript.

Conflicts of interest

Authors declare that they have no conflicts interest.

Data availability

All data collected for this article are presented through figures. However, the data will be made available from the authors upon request.

Supplementary information (SI) is available. See DOI: https://doi.org/10.1039/d5ra08475j.

References

1 D. S. Malik, A. K. Sharma, A. K. Sharma, R. Thakur and M. Sharma, *Advances in Environmental Pollution Management: Wastewater Impacts and Treatment Technologies*, 2020, 1, 10–28.
2 M. Islam, S. Kumar, N. Saxena and A. Nafees, *ChemistrySelect*, 2023, **8**, e202301048.
3 L. Lin, H. Yang and X. Xu, *Front. Environ. Sci.*, 2022, **10**, 880246.
4 R. P. Schwarzenbach, T. Egli, T. B. Hofstetter, U. Von Gunten and B. Wehrli, *Annu. Rev. Environ. Resour.*, 2010, **35**, 109–136.
5 C. M. Cooper, *J. Environ. Qual.*, 1993, **22**, 402–408.
6 S. Madhav, A. Ahamad, A. K. Singh, J. Kushawaha, J. S. Chauhan, S. Sharma and P. Singh, *Sensors in Water Pollutants Monitoring: Role of Material*, 2019, 43–62.
7 P. Dutta, M. Rabbi, M. A. Sufian and S. Mahjebin, *Eng. appl. sci. lett.*, 2022, **5**, 1.
8 R. Al-Tohamy, S. S. Ali, F. Li, K. M. Okasha, Y. A.-G. Mahmoud, T. Elsamahy, H. Jiao, Y. Fu and J. Sun, *Ecotoxicol. Environ. Saf.*, 2022, **231**, 113160.
9 M. Vinuth, H. S. B. Naik, B. M. Vinoda, S. M. Pradeepa, G. A. Kumar and K. C. Sekhar, *J. Environ. Anal. Toxicol.*, 2016, **6**, 1000355.
10 J. A. Buledi, A. Hyder, A. Ali, A. R. Solangi, A. Mallah, S. Amin, A. A. Memon, K. H. Thebo and M. Kazi, *J. Phys. Chem. Solids*, 2024, **192**, 112083.
11 A. Kumar, C. J. Raorane, A. Syed, A. H. Bahkali, A. M. Elgorban, V. Raj and S. C. Kim, *Environ. Res.*, 2023, **216**, 114741.
12 A. Khatri and P. S. Rana, *Phys. B*, 2020, **579**, 411905.
13 F. M. D. Chequer, V. de Paula Venâncio, M. de, L. P. Bianchi and L. M. G. Antunes, *Food Chem. Toxicol.*, 2012, **50**, 3447–3451.
14 W. K. Walthall and J. D. Stark, *Environ. Pollut.*, 1999, **104**, 207–215.
15 N. K. Tripathy, M. J. Nabi, G. P. Sahu and A. A. Kumar, *Food Chem. Toxicol.*, 1995, **33**, 923–927.
16 E. E. Ritchie, J. I. Princz, P. Y. Robidoux and R. P. Scroggins, *Chemosphere*, 2013, **90**, 2129–2135.
17 D. S. Chaudhari, R. P. Upadhyay, G. Y. Shinde, M. B. Gawande, J. Filip, R. S. Varma and R. Zbořil, *Green Chem.*, 2024, **26**, 7579–7655.
18 F. T. Geldasa, M. A. Kebede, M. W. Shura and F. G. Hone, *RSC Adv.*, 2023, **13**, 18404–18442.
19 S. Yadav, K. Shakya, A. Gupta, D. Singh, A. R. Chandran, A. Varayil Aanappalli, K. Goyal, N. Rani and K. Saini, *Environ. Sci. Pollut. Res.*, 2023, **30**, 71912–71932.
20 C. C. Nguyen, N. N. Vu and T.-O. Do, *J. Mater. Chem. A*, 2015, **3**, 18345–18359.
21 S. Chahal, N. Rani, A. Kumar and P. Kumar, *Vacuum*, 2020, **172**, 109075.
22 F. Zhang, X. Wang, H. Liu, C. Liu, Y. Wan, Y. Long and Z. Cai, *Appl. Sci.*, 2019, **9**, 2489.
23 H. Tong, S. Ouyang, Y. Bi, N. Umezawa, M. Oshikiri and J. Ye, *Adv. Mater.*, 2012, **24**, 229–251.
24 G. S. Kamble and Y.-C. Ling, *Sci. Rep.*, 2020, **10**, 12993.
25 R. C. Ghaware, N. B. Birajdar, G. S. Kamble and S. S. Kolekar, *Langmuir*, 2024, **40**, 14426–14439.
26 P. D. Sanadi, R. K. Chougale, D. B. Malavekar, J. H. Kim, S. Masimukku, G.-P. Chang-Chien, Y.-Y. Lee, R. C. Ghaware, S. S. Kolekar and G. S. Kamble, *Spectrochim. Acta, Part A*, 2025, **341**, 126404.
27 Y. Nam, J. H. Lim, K. C. Ko and J. Y. Lee, *J. Mater. Chem. A*, 2019, **7**, 13833–13859.
28 M. T. Noman, N. Amor and M. Petru, *Crit. Rev. Solid State Mater. Sci.*, 2022, **47**, 99–141.
29 P. Rong, S. Ren and Q. Yu, *Crit. Rev. Anal. Chem.*, 2019, **49**, 336–349.
30 D. M. Cruz, E. Mostafavi, A. Vernet-Crua, H. Barabadi, V. Shah, J. L. Cholula-Díaz, G. Guisbiers and T. J. Webster, *J. Phys. Mater.*, 2020, **3**, 34005.
31 A. Kołodziejczak-Radzimska and T. Jesionowski, *Materials*, 2014, **7**, 2833–2881.
32 S. Sharma, M. S. Chauhan, S. Chauhan and S. Kumar, *Next Mater.*, 2025, **7**, 100367.
33 R. Khan, V. Tirth, A. Ali, K. Irshad, N. Rahman, A. Algahtani, M. Sohail and S. Isalm, *J. Mater. Sci.: Mater. Electron.*, 2021, **32**, 21631–21642.
34 X. Jin, Y. Yan, L. Tian and J. Zhang, *Mater. Sci. Semicond. Process.*, 2022, **142**, 106522.
35 F. Islam, S. Shohag, M. J. Uddin, M. R. Islam, M. H. Nafady, A. Akter, S. Mitra, A. Roy, T. Bin Emran and S. Cavalu, *Materials*, 2022, **15**, 2160.
36 J. J. Mahanthe, L. Karunanayake, I. Munaweera, D. A. S. Amarasinghe, K. Dharmapala and H. Imnisar, *J. Rubber Res.*, 2025, 1–17.
37 S. Pramanik, S. Mondal, A. C. Mandal, S. Mukherjee, S. Das, T. Ghosh, R. Nath, M. Ghosh and P. K. Kuiri, *J. Alloys Compd.*, 2020, **849**, 156684.
38 S. Mondal and B. Bhattacharjee, *Emerg. Mater.*, 2025, 1–26.
39 R. Zahoor, A. Jalil, S. Z. Ilyas, S. Ahmed and A. Hassan, *Results Surf. Interfaces*, 2021, **2**, 100003.
40 Z. Mannai, W. Bouslama, I. Karkouch, L. Bouslama, K. Khlifi, K. Aouadi and F. Nouira, *Mater. Chem. Phys.*, 2025, **329**, 130071.
41 N. Mohamed Faizee, C. Joel, R. Imran Khan and M. S. M. Badhusha, *Inorg. Nano-Met. Chem.*, 2025, **55**, 29–38.
42 A. Baig, M. Siddique and S. Panchal, *Catalysts*, 2025, **15**, 100.
43 A. A. Essawy, I. H. Alsohaimi, M. S. Alhumaimess, H. M. A. Hassan and M. M. Kamel, *J. Environ. Manage.*, 2020, **271**, 110961.
44 M. Huston, M. Debella, M. Dibella and A. Gupta, *Nanomaterials*, 2021, **11**, 1–29.
45 I. Hussain, N. B. Singh, A. Singh, H. Singh and S. C. Singh, *Biotechnol. Lett.*, 2016, **38**, 545–560.
46 J. Singh, T. Dutta, K.-H. Kim, M. Rawat, P. Samddar and P. Kumar, *J. Nanobiotechnol.*, 2018, **16**, 84.

47 V. V Makarov, A. J. Love, O. V Sinitsyna, S. S. Makarova, I. V Yaminsky, M. E. Taliansky and N. O. Kalinina, *Acta Nat.*, 2014, **6**, 35.
48 B. Haspulat Taymaz, M. Demir, H. Kamış, H. Orhan, Z. Aydoğan and A. Akıllı, *Int. J. Phytoremediation*, 2023, **25**, 1306–1317.
49 L. M. Jose, R. S. A. Raj, D. Sajan and A. Aravind, *Nano Express*, 2021, **2**, 10039.
50 M. Shabaani, S. Rahaiee, M. Zare and S. M. Jafari, *LWT–Food Sci. Technol.*, 2020, **134**, 110133.
51 M. Alam, *Nanotechnol. Rev.*, 2021, **10**, 1079–1091.
52 M. Golmohammadi, M. Honarmand and S. Ghanbari, *Spectrochim. Acta, Part A*, 2020, **229**, 117961.
53 U. Wijesinghe, G. Thiripuranathar, F. Menaa, H. Iqbal, A. Razzaq and H. Almukhlifi, *Catalysts*, 2021, **11**, 831.
54 F. P. Araujo, P. Trigueiro, L. M. C. Honório, M. B. Furtini, D. M. Oliveira, L. C. Almeida, R. R. P. Garcia, B. C. Viana, E. C. Silva-Filho and J. A. Osajima, *Dalton Trans.*, 2020, **49**, 16394–16403.
55 C. A. Soto-Robles, O. Nava, L. Cornejo, E. Lugo-Medina, A. R. Vilchis-Nestor, A. Castro-Beltrán and P. A. Luque, *J. Mol. Struct.*, 2021, **1225**, 129101.
56 K. Akila, S. Thambidurai, N. Suresh and K. M. Prabu, *Ionics*, 2024, 1–13.
57 M. N. Alharthi, I. Ismail, S. Bellucci, N. H. Khdary and M. Abdel Salam, *Nanomaterials*, 2021, **11**, 1682.
58 D. Zewde and B. Geremew, *Environ. Pollut. Bioavailability*, 2022, **34**, 224–235.
59 K. K. Supin, P. N. PM and M. Vasundhara, *RSC Adv.*, 2023, **13**, 1497–1515.
60 M. N. Zafar, Q. Dar, F. Nawaz, M. N. Zafar, M. Iqbal and M. F. Nazar, *J. Mater. Res. Technol.*, 2019, **8**, 713–725.
61 F. Sako, N. Taniguchi, N. Kobayashi and E. Takakuwa, *Toxicol. Appl. Pharmacol.*, 1977, **39**, 111–117.
62 F. Sako, N. Kobayashi, H. Watabe and N. Taniguchi, *Toxicol. Appl. Pharmacol.*, 1980, **54**, 285–292.
63 S. K. Bhar, S. Jana, A. Mondal and N. Mukherjee, *J. Colloid Interface Sci.*, 2013, **393**, 286–290.
64 M. Farbod and M. Khademalrasool, *Powder Technol.*, 2011, **214**, 344–348.
65 K. Vignesh, R. Hariharan, M. Rajarajan and A. Suganthi, *Solid State Sci.*, 2013, **21**, 91–99.
66 M. I. Khan, M. N. Akhtar, N. Ashraf, J. Najeeb, H. Munir, T. I. Awan, M. B. Tahir and M. R. Kabli, *Appl. Nanosci.*, 2020, **10**, 2351–2364.
67 K. Kumar, M. Chitkara, I. S. Sandhu, D. Mehta and S. Kumar, *J. Alloys Compd.*, 2014, **588**, 681–689.
68 J. Kadam, P. Dhawal, S. Barve and S. Kakodkar, *SN Appl. Sci.*, 2020, **2**, 1–16.
69 S. Mahalingam, J. Ramasamy and Y.-H. Ahn, *J. Taiwan Inst. Chem. Eng.*, 2017, **80**, 276–285.
70 T. Sarkar, S. Kundu, G. Ghorai, P. K. Sahoo and A. Bhattacharjee, *Adv. Nat. Sci.:Nanosci. Nanotechnol.*, 2023, **14**, 35001.
71 T. Sarkar, S. Kundu and A. Bhattacharjee, *Phys. Status Solidi A*, 2024, **221**, 1–13.
72 Z. Khuzwayo and E. M. N. Chirwa, *J. Hazard. Mater.*, 2015, **300**, 459–466.
73 M. Ravbar, A. Kunčič, L. Matoh, S. S. Možina, M. Šala and A. Šuligoj, *RSC Adv.*, 2022, **12**, 31235–31245.
74 K. K. Taha, M. Al Zoman, M. Al Outeibi, S. Alhussain, A. Modwi and A. A. Bagabas, *Nanotechnol. Environ. Eng.*, 2019, **4**, 10.
75 E. Kusiak-Nejman, J. Wojnarowicz, A. W. Morawski, U. Narkiewicz, K. Sobczak, S. Gierlotka and W. Lojkowski, *Appl. Surf. Sci.*, 2021, **541**, 148416.
76 M. Qamar, M. Saquib and M. Muneer, *Desalination*, 2005, **171**, 185–193.
77 R. Velmurugan and M. Swaminathan, *Sol. Energy Mater. Sol. Cells*, 2011, **95**, 942–950.
78 J. P. Shubha, K. Kavalli, S. F. Adil, M. E. Assal, M. R. Hatshan and N. Dubasi, *J. King Saud Univ. Sci.*, 2022, **34**, 102047.
79 I. Kazeminezhad and A. Sadollahkhani, *J. Mater. Sci.: Mater. Electron.*, 2016, **27**, 4206–4215.
80 K. A. Isai and V. S. Shrivastava, *SN Appl. Sci.*, 2019, **1**, 1–11.
81 E. L. Irede, R. F. Awoyemi, B. Owolabi, O. R. Aworinde, R. O. Kajola, A. Hazeez, A. A. Raji, L. O. Ganiyu, C. O. Onukwuli and A. P. Onivefu, *RSC Adv.*, 2024, **14**, 20992–21034.
82 J. Kaur and S. Singhal, *Phys. B*, 2014, **450**, 49–53.
83 S. Alkaykh, A. Mbarek and E. E. Ali-Shattle, *Heliyon*, 2020, **6**, e03663.
84 Y. Nosaka and A. Nosaka, *ACS Energy Lett.*, 2016, **1**, 356–359.
85 M. D. Nasikhudin, A. Kusumaatmaja and K. Triyana, in *Journal of Physics: Conference Series*, IOP Publishing, 2018, vol. **1011**, p. 12069.
86 M. Zhang, X. Liu, X. Zeng, M. Wang, J. Shen and R. Liu, *Chem. Phys. Lett.*, 2020, **738**, 100049.
87 M. Siddique, N. M. Khan, M. Saeed, S. Ali and Z. Shah, *Z. Phys. Chem.*, 2021, **235**, 663–681.
88 S. Kundu, T. Sarkar, A. A. Al-Ahmadi, E. Ali and A. Bhattacharjee, *RSC Adv.*, 2024, **14**, 28944–28955.
89 T. Sarkar, S. Kundu, G. Ghorai, P. K. Sahoo and A. Bhattacharjee, *Part. Part. Syst. Char.*, 2024, **41**, 2400073.
90 Y.-W. Chen and Y.-H. Hsu, *Catalysts*, 2021, **11**, 966.
91 F. Meng, Y. Liu, J. Wang, X. Tan, H. Sun, S. Liu and S. Wang, *J. Colloid Interface Sci.*, 2018, **532**, 321–330.
92 M. Janus, E. Kusiak-Nejman and A. W. Morawski, *React. Kinet. Mech. Catal.*, 2012, **106**, 289–295.
93 Y. Meng, S. Xia, G. Pan, J. Xue, J. Jiang and Z. Ni, *Korean J. Chem. Eng.*, 2017, **34**, 2331–2341.
94 Y. D. Kaldante, R. N. Shirsat and M. G. Chaskar, *Nanosyst.: Phys. Chem. Math.*, 2021, **12**, 773–782.
95 V. Archana, J. Joseph Prince and S. Kalainathan, *J. Nanomater.*, 2021, **2021**, 1–25.
96 S. Chahal, N. Rani, A. Kumar and P. Kumar, *Appl. Surf. Sci.*, 2019, **493**, 87–93.
97 I. Kir, S. E. Laouini, S. Meneceur, A. Bouafia and H. A. M. Mohammed, *Biomass Convers. Biorefin.*, 2023, 1–10.
98 C. Baumanis, J. Z. Bloh, R. Dillert and D. W. Bahnemann, *J. Phys. Chem. C*, 2011, **115**, 25442–25450.

99 G. G. Hasan, H. A. Mohammed, M. Althamthami, A. Khelef, S. E. Laouini and S. Meneceur, *J. Photochem. Photobiol., A*, 2023, **443**, 114874.
100 H. Singh, S. Kumar, H. Kaur, J. Gaur, Supreet, G. Singh, M. Kaur, S. Kumar, R. Pal and N. Kaur, *Interactions*, 2024, **245**, 183.
101 L. M. Verma, A. Kumar, A. U. Bashir, U. Gangwar, P. P. Ingole and S. Sharma, *Nanoscale Adv.*, 2024, **6**, 155–169.
102 R. Yanagi, T. Zhao, D. Solanki, Z. Pan and S. Hu, *ACS Energy Lett.*, 2021, **7**, 432–452.